Article

Rational Design of Mononuclear Iron-porphyrins for Facile and Selective 4e⁻/4H⁺ O₂ Reduction: Activation of O-O Bond by 2nd Sphere Hydrogen Bonding

Sarmistha Bhunia, Atanu Rana, Pronay Roy, Daniel J. Martin, Michael L. Pegis, Bijan Roy, and Abhishek Dey

J. Am. Chem. Soc., **Just Accepted Manuscript** • Publication Date (Web): 05 Jul 2018

Rational Design of Mononuclear Iron-porphyrins for Facile and Selective $4e^-/4H^+$ O_2 Reduction: Activation of O-O Bond by 2nd Sphere Hydrogen Bonding

Sarmistha Bhunia[1], *Atanu Rana*[1], *Pronay Roy*[1], *Daniel J. Martin*[2,‖], *Michael L. Pegis*[2,3,‖], *Bijan Roy*[1], *Abhishek Dey**[,1]

[1]Department of Inorganic Chemistry, Indian Association for the Cultivation of Science, 2A Raja SC Mullick Road, Kolkata, West Bengal, India 700032

[2]Department of Chemistry, Yale University, New Haven, Connecticut 06520, United States

[3]Department of Chemistry, Massachusetts Institute of Technology, Cambridge, Massachusetts 02139, United States

‖ equal contribution

Email: icad@iacs.res.in

Abstract

Facile and selective $4e^-/4H^+$ electrochemical reduction of O_2 to H_2O in aqueous medium has been a sought-after goal for several decades. Elegant but synthetically demanding cytochrome c oxidase mimics have demonstrated selective $4e^-/4H^+$ electrochemical O_2 reduction to H_2O is possible with rate constants as fast as 10^5 $M^{-1}s^{-1}$ under heterogeneous conditions in aqueous media. Over the last few years, in-situ mechanistic investigations on iron porphyrin complexes adsorbed on electrodes have revealed that the rate and selectivity of this multi-electron and multi-proton process is governed by the reactivity of a ferric hydroperoxide intermediate. The barrier of O-O bond cleavage determines the overall rate of O_2 reduction and the site of protonation determines the selectivity. In this report, a series of mononuclear iron porphyrin complexes are rationally designed to achieve efficient O-O bond activation and site-selective proton transfer to effect facile and selective electrochemical reduction of O_2 to water. Indeed, these crystallographically characterized complexes accomplish facile and selective reduction of O_2 with rate constants $>10^7$ $M^{-1}s^{-1}$ while retaining >95% selectivity when adsorbed on electrode surfaces (EPG) in water. These ORR rate constants are two orders of magnitude faster than all known heme/Cu complexes and these complexes retain >90% selectivity even under rate determining electron transfer conditions which generally can only be achieved by installing additional redox active groups in the catalyst.

Introduction

The reduction of molecular oxygen (O_2) to water is a fundamental process in nature and is key to a sustainable fuel cell technology.[1-3] Whereas the reduction of O_2 to H_2O requires $4e^-$ and $4H^+$, the delivery of insufficient number of electrons and/or protons results in the generation of partially reduced oxygen species (PROS) like superoxide, peroxide and hydroxyl radical, all of which are very reactive and detrimental to chemical and biological systems.[4,5] In nature, Cytochrome c oxidase (CcO) catalyses the selective $4e^-/4H^+$ reduction of oxygen to water during respiration in all aerobic organisms and drives the mechano-chemical synthesis of ATP.[6,7,8] CcO is a member of the heme-Cu oxidase family and its active site comprises of a bimetallic copper/heme core supported by histidine residues and a Tyr244 residue (Figure 1A).[9,10] There are two electron transfer heme sites (heme a and heme a_3) and these along with the Cu_B site provides the electrons necessary for the $4e^-/4H^+$ reduction of O_2 in the reduced state.[11,12] The Tyr244 residue can act as an electron donor when the heme a and Cu_A sites are not reduced (i.e., in the mixed valent state).[13-15] The protons required for the process, on the other hand, are delivered into the active site of this membrane protein via defined proton channels.[11,12]

O_2 reduction by synthetic metallo-porphyrins have been rigorously studied in aqueous conditions using heterogeneous electrochemistry.[16-20] Under such conditions, unlike the heme/Cu site of CcO, mononuclear iron porphyrin catalysts (even cobalt analogues under acidic conditions) typically reduce O_2 by $2e^-/2H^+$ to H_2O_2 and produce very little water.[21-23] Only by including electron donating residues in the distal site, $4e^-/4H^+$ reduction can be achieved.[24,25] Thus the finesse of cytochrome c oxidase has been difficult to emulate in synthetic systems. Over the last several decades several groups have attempted to emulate the reactivity of the heme/Cu site of CcO by designing elaborate synthetic and functional models of CcO. These analogues also established the importance of the Cu_B and Tyr244 residues in enhancing the selectivity of the $4e^-/4H^+$ process over the $2e^-/2H^+$ reduction of O_2 under heterogeneous aqueous conditions.[26-35] Bio-synthetic models including the tyrosine residues have been shown to reduce O_2 to H_2O selectively both in solution as well as when adsorbed on electrodes.[36,37] In parallel, small synthetic complexes inspired by the working principles of the heme/Cu site in CcO were fashioned with the goal of effecting $4e^-/4H^+$ reduction of O_2. For example, a series of cobalt hangman porphyrins bearing proton transfer pendent carboxylic acid residues were found to selectively (70%) promote the $4e^-/4H^+$ reduction in acidic water

medium.[22] Other reports have shown that redox active ferrocene groups and distal hydrogen bonding environments both at the distal site can also improve selectivity in aqueous media across a wide pH range.[19,38] The enhanced selectivity has been achieved for more extended water networks of the oxygen bound 2-pyridyl substituted porphyrins by Mayer and his co-workers as well.[21,39,40] The stability of the catalysts along with the selectivity has also been established on EPG and BPG electrodes under acidic heterogeneous condition having proton relay groups (pyridine, carboxylic acid and hydroxyl phenyl) in one meso position of asymmetric iron porphyrins.[41] A strong hydrogen bonding network exists, and is crucial for reactivity, in the active site of horseradish peroxidase (HRP) where a distal "pull effect" is known to enhance the rate of O-O bond cleavage of a ferric hydroperoxide (compound 0) intermediate (Figure 1B).[42,43]

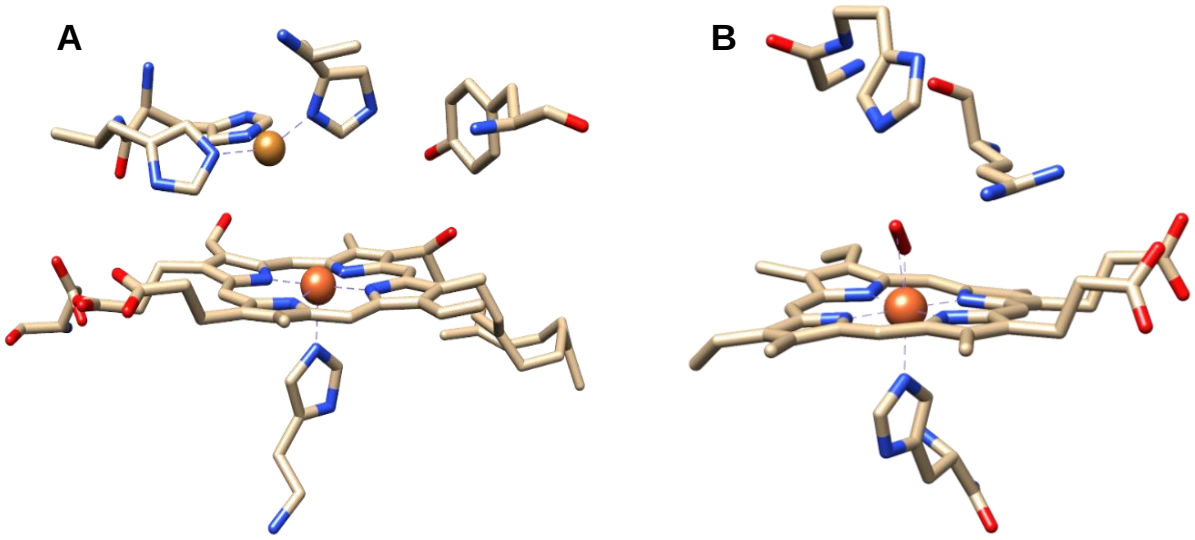

Figure 1. Binuclear active site structure of CcO (PDB ID: 1OCC)[10] (A), HRP (compound III), active site structure (PDB ID: 1H57) (B).[44] color codes: carbon → offwhite, nitrogen → blue, oxygen → red, iron → brown and Copper → golden yellow . Hydrogen atoms are omitted in the crystal structures for clarity.

The competing kinetic steps that lead to product bifurcation (H_2O vs H_2O_2) have been historically challenging to prove, especially for complexes adsorbed on electrodes. Recently, Surface Enhanced Resonance Raman coupled to Rotating Disc Electrochemistry (SERRS-RDE) has enabled in-operando identification of reactive intermediates under catalytic steady state.[45,46-48] The results suggest that for iron porphyrins with neutral axial ligands (e.g., imidazole, water etc.) a low spin Fe^{III}-OOH species is produced on the electrode. The O-O bond of this species is quite strong (~820-830 cm^{-1}) and can only be cleaved after this species

is reduced by one electron (i.e., to Fe^{II}-OOH) or transformed to a Fe^{IV}=O species via a proton coupled electron transfer (PCET).[46,49] Protonation of the proximal oxygen leads to hydrolysis and releases H_2O_2 (Scheme 1).[50,51] The rate of hydrolysis is fast and has a H_2O/D_2O isotope effect of 4.5. Under the circumstances where the rate of electron transfer from the electrode is slow, the competing hydrolysis steps predominate resulting in more $2e^-/2H^+$ reduction of O_2 to form H_2O_2.[52] Logically, when the rate of electron transfer to these intermediates are reduced (slow electron flux from the electrode), the hydrolysis of the hydroperoxide as well as superoxide species eventually produces ROS (scheme 1). Similar conclusions have been deduced using cyclic voltammetry (CV) simulation and stopped flow kinetics for homogeneous O_2 reduction by iron porphyrins in organic solutions.[53,54] Alternatively, protonation of the Fe^{III}-OOH distal oxygen by 2nd sphere proton donors can lead to O-O bond cleavage without having to reduce it (Scheme 1), as has been observed for natural enzymes like peroxidases.[43,54-56] In peroxidases, a distal basic residue, which is protonated at physiological pH, can activate the O-O bond of Fe^{III}-OOH via hydrogen bonding, termed as the pull effect.[42,43,57] The pull effect of protonated basic residues has not yet been emulated in synthetic systems involved in ORR although the effect of strong electrostatic interaction is clearly demonstrated in CO_2 reduction.[58] If oriented correctly, distal residues that can H-bond with the distal oxygen atom of Fe^{III}-OOH could stabilize the intermediate against hydrolysis, activate the O-O bond, and facilitate the selective reduction of O_2 to water.[59] All of the previous reported examples of mononuclear Fe porphyrins, without appended redox cofactors e.g., Cu, ferrocene (Fc) have been investigated for the influence of properly positioned proton donors which work under acidic conditions.[22] A highly efficient and selective model operable at neutral pH has not been discovered so far which contains the proton relay motif that can operate near neutral pH.

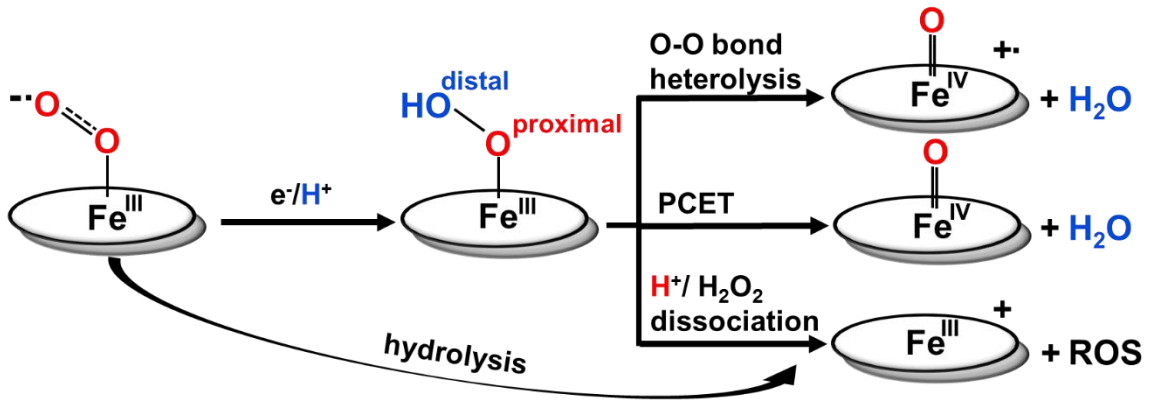

Scheme 1. Schematic representation of the factors determining the $2e^-/2H^+$ vs $4e^-/4H^+$ selectivity in O_2 reduction by iron porphyrin complexes. [The oval ring represents the

porphyrin ligand; red and blue color denotes the proximal and distal oxygen atoms of a bound hydroperoxide ligand, respectively.]

In this manuscript, we prepare a new series of iron porphyrin complexes containing basic residues above the active sites and investigate their performance as ORR electrocatalysts. The data demonstrate that inclusion of basic residues in the distal site of mononuclear iron porphyrins allow facile and selective $4e^-/4H^+$ reduction of O_2 to water in pH 7 buffer when adsorbed on EPG electrodes. These tailor-made iron porphyrin complexes are crystallographically characterised and the electrocatalytic O_2 reduction data reveal rate constants (second order) that exceed state-of-the-art CcO model systems by two orders of magnitude while producing >90% H_2O as a product, even under very slow rates of interfacial electron transfer. Computational modelling suggests that installation of the pendant bases provides hydrogen-bond assisted stabilization and activation of the Fe^{III}-OOH intermediates in the catalytic cycle. Consequentially, these motifs facilitate selective protonation of the distal oxygen in Fe^{III}-OOH before further reduction, providing unprecedented $4e^-/4H^+$ selectivity in adsorbed mononuclear iron porphyrin complexes. These results demonstrate how the "pull effect" observed in peroxidases can be emulated to enable enhanced ORR activity that rivals CcO in simple mononuclear iron porphyrin electrocatalysts.

Results

i. Synthesis

The synthetic strategy utilized *o*-aminophenyl-tris(phenyl)-porphyrin (**MATPP**) as the common starting material.[60] The synthesis of ligand **L1** (1d) requires dialkylation of ZnMAPP (1b) with benzyl bromide and triethylamine at room temperature followed by demetallation under acidic condition (dil. HCl) (A, Scheme 2). The ligand **L2** (2a) was synthesized by Schiff-base condensation of the aromatic amine with pyridine-2-carboxaldehyde using trifluoroacetic acid (TFA) as a catalyst at room temperature prior to imine reduction using $NaBH_4$ (B, Scheme 2). Again, starting from MAPP, monoalkylation of the aromatic amine is done with 2-bromo-ethylamine hydrobromide and catalytic amounts of TBAI (tetrabutylammonium iodide) in toluene under reflux condition to prepare ligand **L3** (3a; C, Scheme 2). All ligands were metallated with iron (ferrous bromide) or zinc acetate using standard protocols.[38,61] The synthetic procedures mentioned above are described in detail in the experimental section (Scheme 2: A, B and C). These ligands and metal complexes were characterised using ESI-MS, ^{1}H-NMR, absorption spectroscopy (UV-Visible) and elemental analysis.

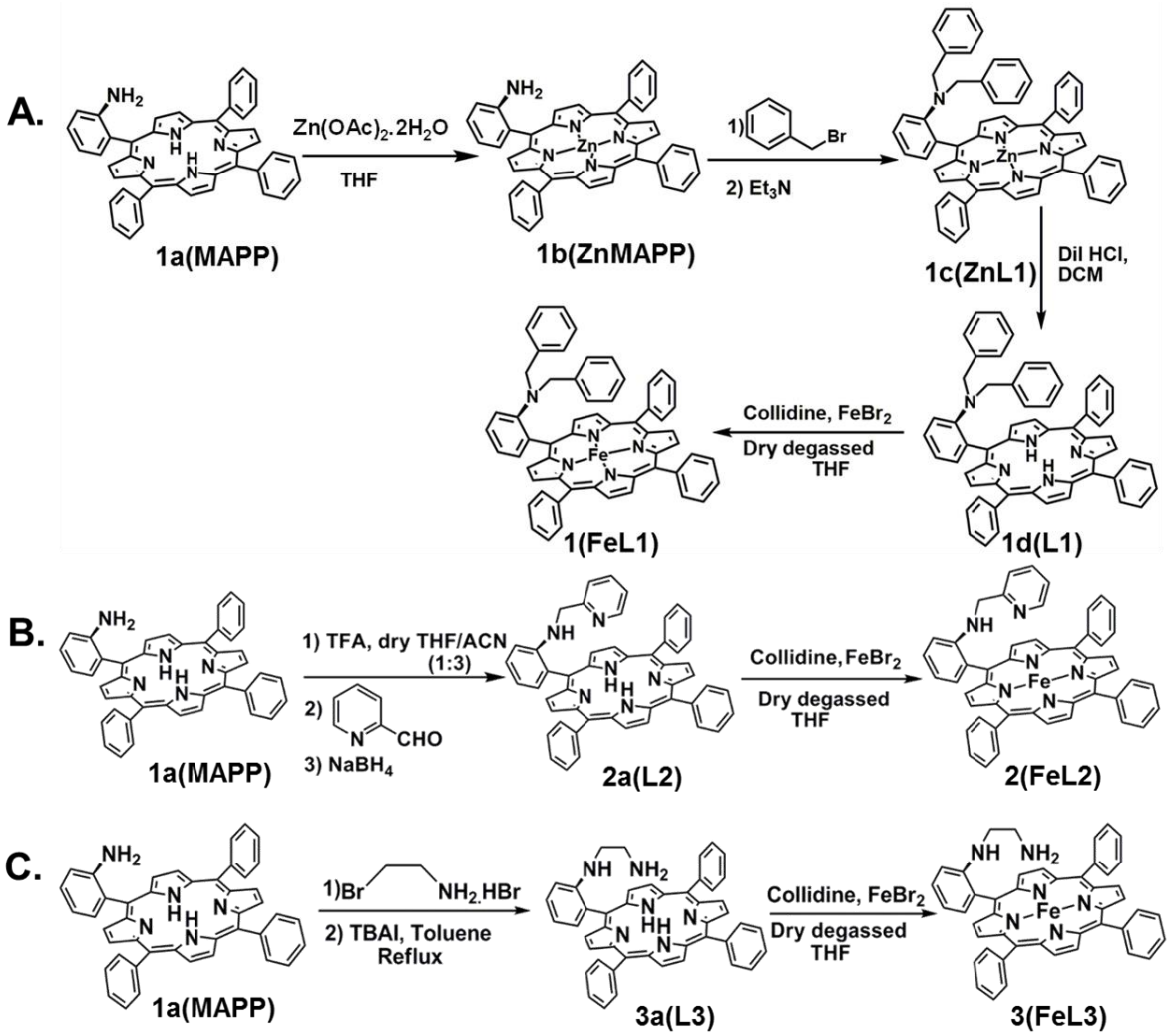

Scheme 2. The synthetic scheme of desired complexes [FeL1(A), FeL2(B) and FeL3(C)].

The solid-state structures of the metallated complexes ($Zn^{II}L1$, $Zn^{II}L2$ and $[Fe^{II}L3(CO)]_2$) were characterized by single crystal X-ray diffraction (SCXRD). Single crystals of ZnL1 (purple colour, *C*c space group, Figure 2A) were obtained by slow evaporation of acetone. Slow diffusion of methanol into a chloroform solution of ZnL2 produced purple needle shaped crystals with a *P*1 space group (Figure 2B). Dark red, needle shaped crystals of the $[FeL3(CO)]_2$ complex were grown under inert atmosphere from the CO saturated THF solution with a space group *P*2/n (Figure 2C). At first 2M solution of FeL3 in THF-MeOH (1:1) solvent mixture was reduced by 0.5eq Na_2S and purged with CO gas for 5 minutes. The solution turned deep red in colour and kept in a closed tube under argon atmosphere.

While both ZnL1 and ZnL2 exist as mononuclear complexes in their crystal structures, $Fe[L3(CO)]_2$ crystalized as a dimer. All three complexes contain the metal ion at the porphyrin plane and the metal ions are coordinated with solvent molecules like acetone and water for

ZnL1 and ZnL2 respectively or CO molecule in the axial positions for FeL3. In addition, for $[FeL3(CO)]_2$, the sixth coordination site of Fe(II) is occupied with $–NH_2$ group of a second Fe-porphyrin unit, forming the dimeric structure. The unique dimeric complex acquires a bowl-shaped architecture which holds a THF molecule inside its hydrophobic cavity. The relevant bond distances for all the crystal structures are summarized in the table below (Table S1) and all other parameters are tabulated in the supporting information (Table S2).

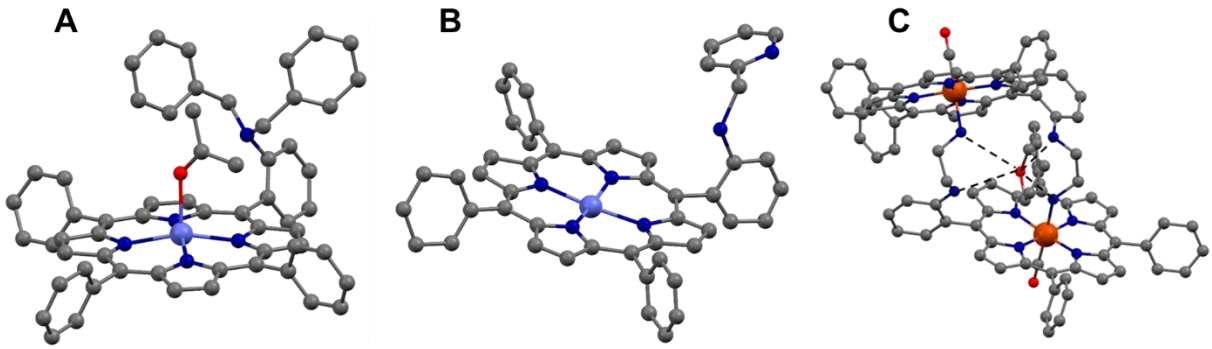

Figure 2. Molecular structures of **ZnL1 (A)**, **ZnL2 (B)** and **FeL3 (C)**. C (grey), N (blue), O (red), Zn (Violet) and Fe (orange). Hydrogen atoms omitted for clarity.

ii. Electrocatalytic O_2 reduction at pH 7

The complexes **FeL1**, **FeL2** and **FeL3** were physiadsorbed on edge-plane graphite (EPG) electrodes and analysed under aqueous conditions at pH 7. In the presence of 1 atm N_2, **FeL1**, **FeL2** and **FeL3** display chemically reversible $Fe^{III/II}$ redox process at -260 mV, -280 mV and -285 mV vs Ag/AgCl (satd. KCl) respectively (Figure S2A). By integrating these redox waves, the surface coverages of **FeL1**, **FeL2** and **FeL3** were found to be $(8.10 \pm 0.52)\times10^{-12}$, $(5.61 \pm 0.15)\times10^{-12}$ and $(1.09 \pm 0.30)\times10^{-11}$ mol/cm^2 respectively. In aerated buffer solutions at pH7 these complexes show electrocatalytic O_2 reduction. Linear sweep voltammetry (LSV) of these catalysts show a substrate diffusion limited catalytic O_2 reduction current with an onset of ≈ -100 mV vs Ag/AgCl (satd. KCl) (Figure 3A, 3C and 3E), indicative of mass transfer limited O_2 reduction. The $E_{1/2}$ of catalysis for FeL1, FeL2 and FeL3 were determined from the maxima of the 1st derivative of ORR current (Table 2). The kinetics and selectivity of O_2 reduction were determined with RDE using Koutecky–Levich (K-L) analysis. In a rotating disc electrochemistry (RDE) experiment, the O_2 reduction current increases with increasing rotation rates following the Koutecky–Levich equation given below:

$$i^{-1} = i_K(E)^{-1} + i_L^{-1} \qquad (1)$$

where, $i_K(E) = nFA[O_2]k_{cat}\Gamma_{catalyst}$, (2)

and $i_L = 0.62nFA[O_2](D_{O2})^{2/3}\omega^{1/2}v^{-1/6}$ (3)

where n is the number of electrons transferred to the substrate, F is the faraday constant, A is the macroscopic area of the disc (0.096 cm^2), $[O_2]$ is the concentration of O_2 in an air saturated buffer (0.21 mM) at 25 ^oC, k_{cat} is the 2nd order rate constant of catalytic O_2 reduction, $\Gamma_{catalyst}$ is the catalyst surface coverage in moles/cm^2, D_{O2} is the diffusion coefficient of O_2 (1.96 x 10^{-5} cm^2 s^{-1}) at 25 ^oC, ω is the angular velocity of the disc and v is the kinematic viscosity of the solution (0.009 cm^2 s^{-1}) at 25 ^oC.[62] When inverse current (i^{-1}) is plotted versus inverse square root of rotation rate ($\omega^{-1/2}$) at -450 mV vs Ag/AgCl (satd. KCl), the slopes are linear and close to those expected for selective 4e$^-$ reduction of O_2 (Figure 3B, D and F). The 2nd order rate constant of electrocatalytic O_2 reduction can also be calculated from K-L plot using the formula

$i_K(E) = nFA[O_2]k_{cat}\Gamma_{catalyst}$ (4)

The k_{cat} values obtained on EPG electrode surface for the complexes **FeL1**, **FeL2** and **FeL3** are $(7.28\pm0.02)\times10^6$ $M^{-1}s^{-1}$, $(1.80\pm0.07)\times10^7$ $M^{-1}s^{-1}$ and $(1.35\pm0.09)\times10^7$ $M^{-1}s^{-1}$, respectively (Table 1). The measured 2nd order rate constants are two orders of magnitude greater than the values reported for heme/Cu model complexes of CcO and are comparable to those of CcO biosynthetic models.[28,45]

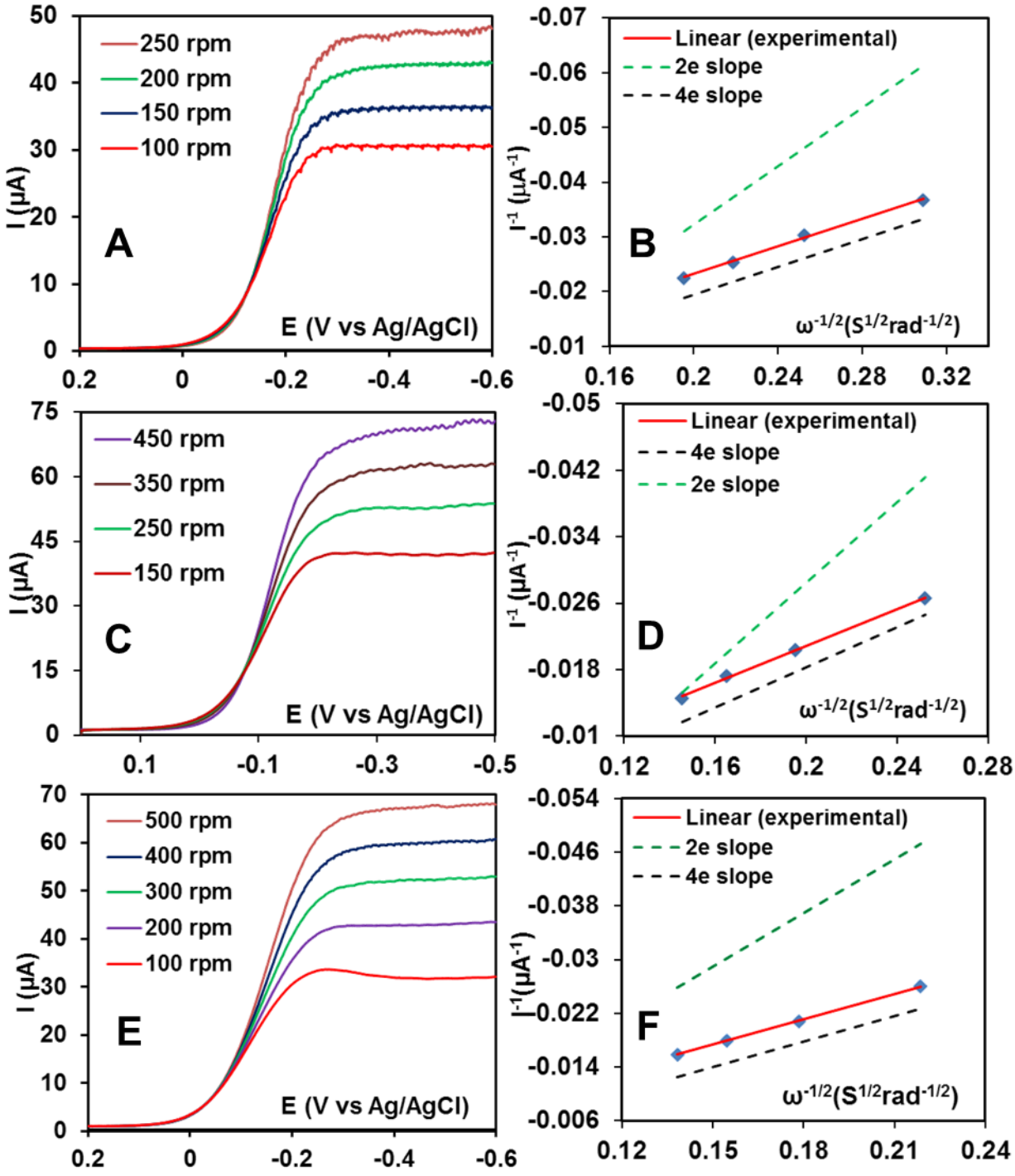

Figure 3. LSV of A) **FeL1** C) **FeL2** E) **FeL3** physiadsorbed on EPG in air saturated pH7 buffer at a scan rate of 100 mV/s at multiple rotations using Ag/AgCl (satd. KCl) reference and Pt wire as counter electrode. K-L plot of B) **FeL1** D) **FeL2** F) **FeL3** at a potential of -450 mV is given and the theoretical plots for $2e^-$ and $4e^-$ processes are indicated in the figure.

The selectivity for O_2 reduction was more accurately quantified by monitoring ROS formation via rotating ring disc electrochemistry (RRDE) (Figure 4, S3 and S6). In a RRDE experiment, any reactive oxygen species (ROS), like O_2^- and H_2O_2, produced at the working electrode is hydrodynamically cast across a surrounding Pt ring encircling the working electrode. The Pt ring is held at a fixed potential (0.7 V at pH7) such that it oxidizes the ROS back to O_2 and generates an oxidative current. The ratio of ring to disk current is a direct measure of the amount of ROS generated in-situ and can be used to measure product selectivity.

The rate of ET from the electrode to the catalyst can also be controlled by immobilizing these catalysts atop self-assembled monolayers (SAM) of thiols having different chain lengths on Au electrodes. Electron transfer rate constants for standard EPG electrodes are as high as ~10^5 s^{-1} whereas octanethiol SAM (C_8-SH) show rate constants of 10^3 s^{-1} and hexadecandethiol SAM (C_{16}-SH) show rates of 6-10 s^{-1}.[29,30,63] The amount of ROS produced by **FeL1** at pH 7 under fast (EPG), moderate (C_8-SH SAM) and slow (C_{16}-SH SAM) electron transfer flux are (2.30±0.20)%, (6.15±0.30)% and (10.45±0.90)%, respectively. Under the same conditions, **FeL2** produces (1.25±0.05)%, (5.20±0.30)%, and (4.90±0.50)% ROS (Figure 4) and **FeL3** produces (2.00±0.10)%, (5.10±0.30)%, and (4.00±0.50)% ROS (Table 2) in EPG, C_8-SH SAM and C_{16}-SH SAM respectively measured from RRDE experiment. The percent of generated ROS remains almost the same for all these complexes and is independent of the electron transfer rate from the electrode. All these mononuclear iron porphyrins require electrons from the electrode to complete the oxygen reduction cycle as at most two electrons can be obtained from reduced ferrous porphyrin centre itself. In the absence of facile electron transfer from the electrode (i.e., under slow electron flux), reaction intermediates like Fe^{III}-O_2^- and Fe^{III}-OOH persist that undergo hydrolysis to generate ROS i.e., catalyze $2e^-/2H^+$ ORR. Thus the selectivity exhibited by this series of complexes is in stark contrast to all previous reports of heterogeneous electrochemical O_2 reduction by mononuclear iron porphyrin complexes (e.g., FeTPP) without any additional redox centres (e.g., distal Cu, ferrocene, or phenol), all of which produce as much as 50-100% ROS on C_{16}-SH SAM which often lead to rapid catalyst degradation.[29,25,4,64] Even under similar conditions of similar electron flux, these mononuclear iron porphyrin complexes are over 90% selective for $4e^-/4H^+$ O_2 reduction to H_2O like the FeCu-CcO model (Table 1).

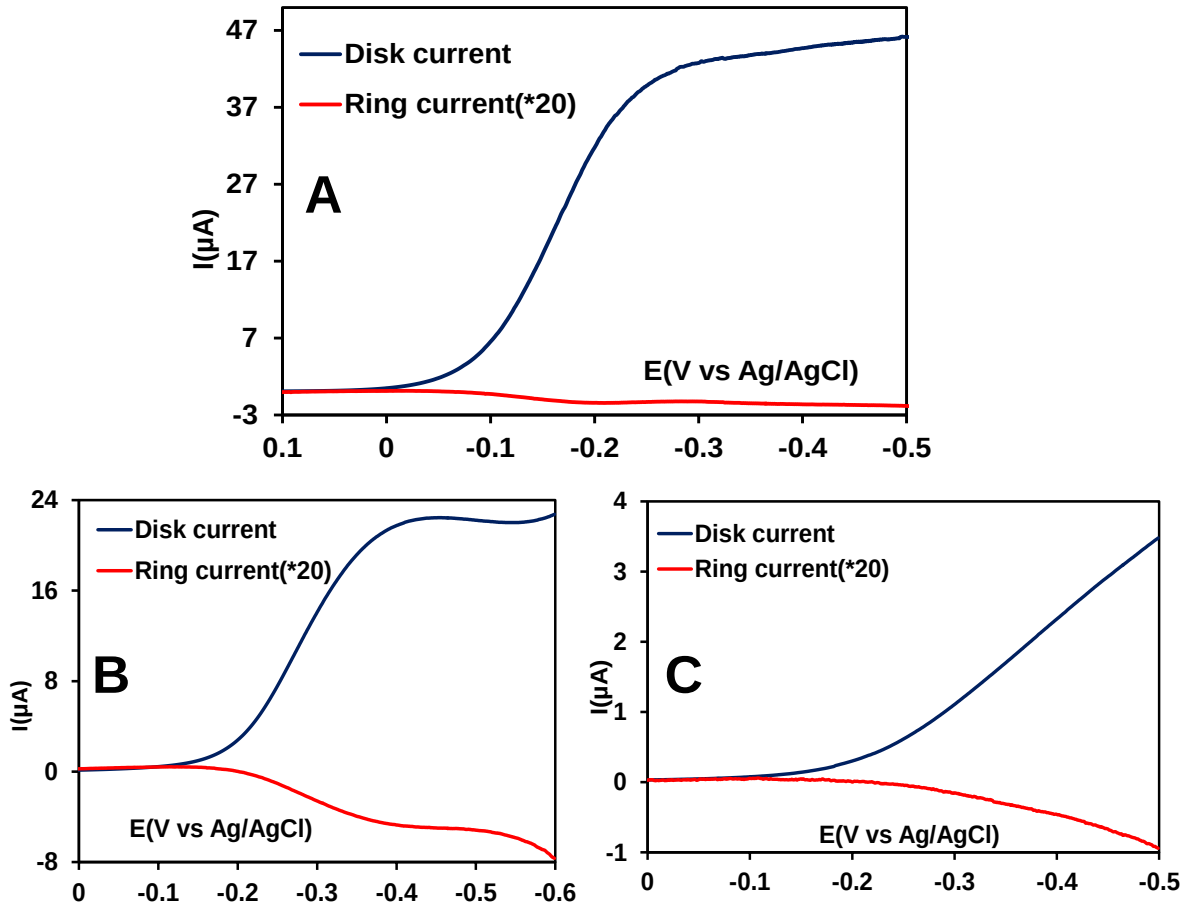

Figure 4. RRDE data of **FeL2** immobilized on EPG, C_8-SH SAM and C_{16}-SH SAM at pH 7, at 100 mV/s scan rate at 300 rpm rotation rate using a Pt counter electrode and Ag/AgCl (satd. KCl) as reference electrode.

The experimental data clearly demonstrate unprecedented selectivity and rate of O_2 reduction for FeL1, FeL2, and FeL3. Most importantly, the selectivity for $4e^-/4H^+$ reduction is maintained even under slow ET conditions. Based on the current mechanistic understanding, the enhanced selectivity maintained even under slow ET implies stabilization of formed Fe^{III}-OOH and Fe^{III}-O_2^- species (Figure S13, 8). The distal-site basic residues are hypothesized to account for this stabilization by hydrogen bonding with these intermediates and retarding their rates of hydrolysis.[59] The enhanced rates also suggest O-O bond activation by the 2nd sphere distal residues. Moreover, the selectivity suggests selective proton transfer to the distal oxygen atom of the Fe^{III}-OOH intermediate. These effects may also affect rates of homogeneous ORR and are evaluated below.

Table 1 : Electrochemical ORR data

Catalyst	$E_{cat/2}$ (mV vs Ag/AgCl)	k_{cat}(× 10^7) ($M^{-1}s^{-1}$)[f]	TOF (s^{-1})[f]	ROS analysis (%)		
				EPG (10^5 s^{-1})[e]	C_8SH (10^3 s^{-1})[e]	$C_{16}SH$ (6-10 s^{-1})[e]
Fe-L1	-155[a]	0.728±0.02	1601	2.30±0.2[c]	6.15±0.30[c]	10.45±0.90[d]
Fe-L2	-103[a]	1.80±0.07	3960	1.25±0.05[c]	5.20±0.30[c]	4.90±0.50[d]
Fe-L3	-105[a]	1.35±0.09	2970	2.00±0.10[c]	5.10±0.30[c]	4.00±0.50[d]
FeTPP	-320[a]	ND[g]	ND[g]	10	29	Rapid degradation
Fe(4-NMePy)[h]	-95	ND	780	60[b]	ND	ND
Fe only CcO[i]	-30[b]	0.005	11.22	ND	10	>20
FeCu[i]	-30[b]	0.012	26.4	ND	7.7	11

a. Obtained from maxima of 1st derivative of ORR catalytic current, b. ORR onset potential c. determined at the potential where the ring current is maximum, d. determined at -200 mV vs NHE, e. Standard rate of electron transfer, f. determined on EPG electrode, g. FeTPP is not stable enough for the determination of the k_{cat}, h. All the data given here are from reference 51, i. References 28 and 30 correspond to all the electrochemical parameters of these two compounds, ND: No mention in their corresponding references. The structures of compounds (h,i) mentioned in this table from other references are given in **Figure 5**.

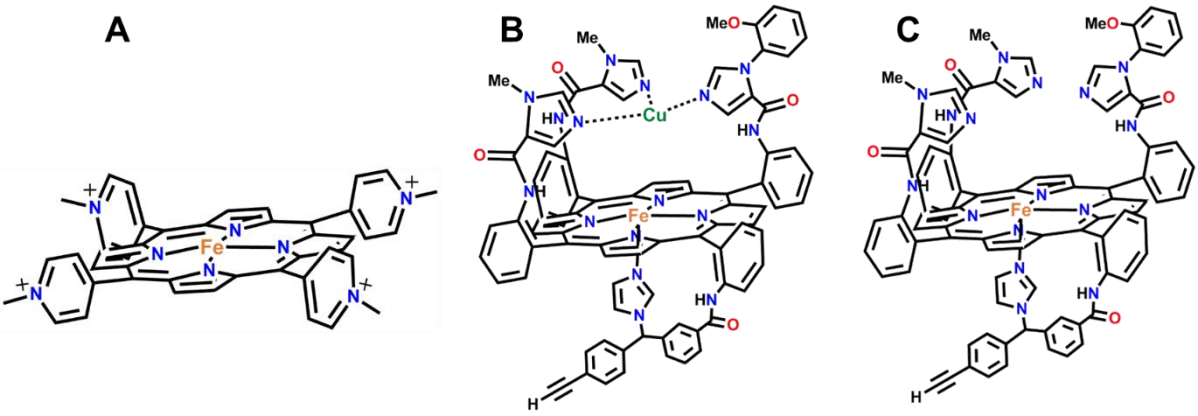

Figure 5. A) FeTMPyP; B) Fe only and C) FeCu heme/Cu oxidase model.

iii. Electrocatalytic O_2 Reduction in DMF

Homogeneous ORR electrocatalysts for Complexes **FeL1**, **FeL2** and **FeL3** were also investigated in DMF solutions under conditions identical to those reported by Mayer and co-workers.[65] In the absence of O_2 and after halide abstraction, chemically reversible Fe(III/II) couples ($E_{1/2}$) were observed at potentials of –545, -502, -531 mV vs $Fc^{+/0}$ for **FeL1**, **FeL2** and **FeL3**, respectively (Figure S9). In the presence of O_2 and the strong acid [DMF-H]OTf, all three catalysts showed irreversible current responses upon sweeping the potential past the Fe(III/II) redox couple, indicative of oxygen reduction electrocatalysis (Figure S10). The first order rate constants for O_2 reduction (k_{obs}) were quantified using the foot-of-the-wave analysis and all catalysts demonstrated first order dependences (Figure S11) on the concentration of $[DMF\text{-}H]^+$ dissolved in solution. We note that, unlike the *heterogeneous* results shown above/below, these catalysts slightly break away from the *homogeneous* TOF:overpotential correlations previously demonstrated by Mayer (Figure 6).[66] However, the efficiency of ORR electrocatalysts is highly dependent on the conditions of study[67],[68] and previous results have demonstrated how the activity of electrode-adsorbed ORR catalysts differs significantly from the same catalysts dissolved in solutions.[21,53] Density functional theory calculations (below) were used to probe the nature of the hydrogen bonding interactions with putative Fe^{III}-O_2^- and Fe^{III}-OOH species.

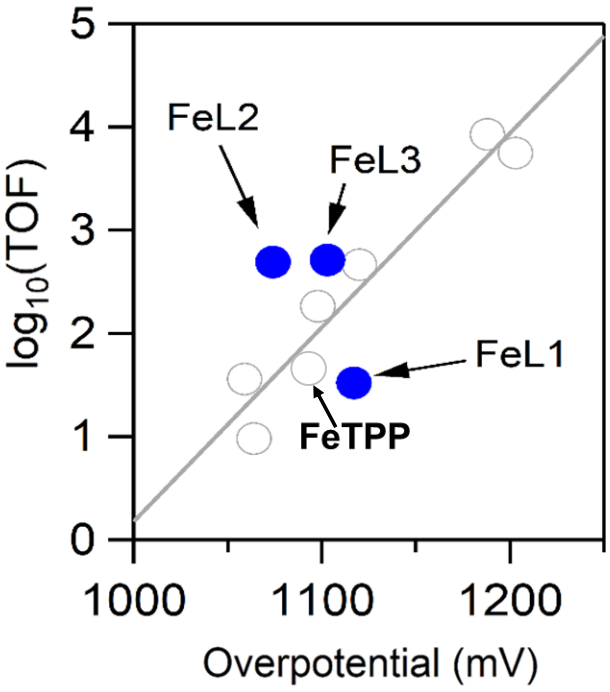

Figure 6. log(TOF) as a function of the catalyst-specific effective overpotential η_{eff} with 50mM [DMF-H]OTf under 1 atm O_2 in 0.1 M [^{n}Bu$_4$N][PF_6] DMF solution. The compounds (**FeL1**, **FeL2** and **FeL3**) studied here are represented by filled blue circles and the empty circles indicate the compounds reported by Mayer and coworkers under same conditions.

iv. DFT Calculations

Density functional theory (DFT) optimized structures were obtained for hypothetical models of FeL1, FeL2, and FeL3 low spin superoxides and hydroperoxides containing axial water ligand. To understand potential hydrogen bonding interactions with the basic residues, Fe^{III}-O_2^- and Fe^{III}-OOH species with neutral basic residues are considered first. Note that this state is unlikely to exist at pH 7 or in the presence of protonated DMF.

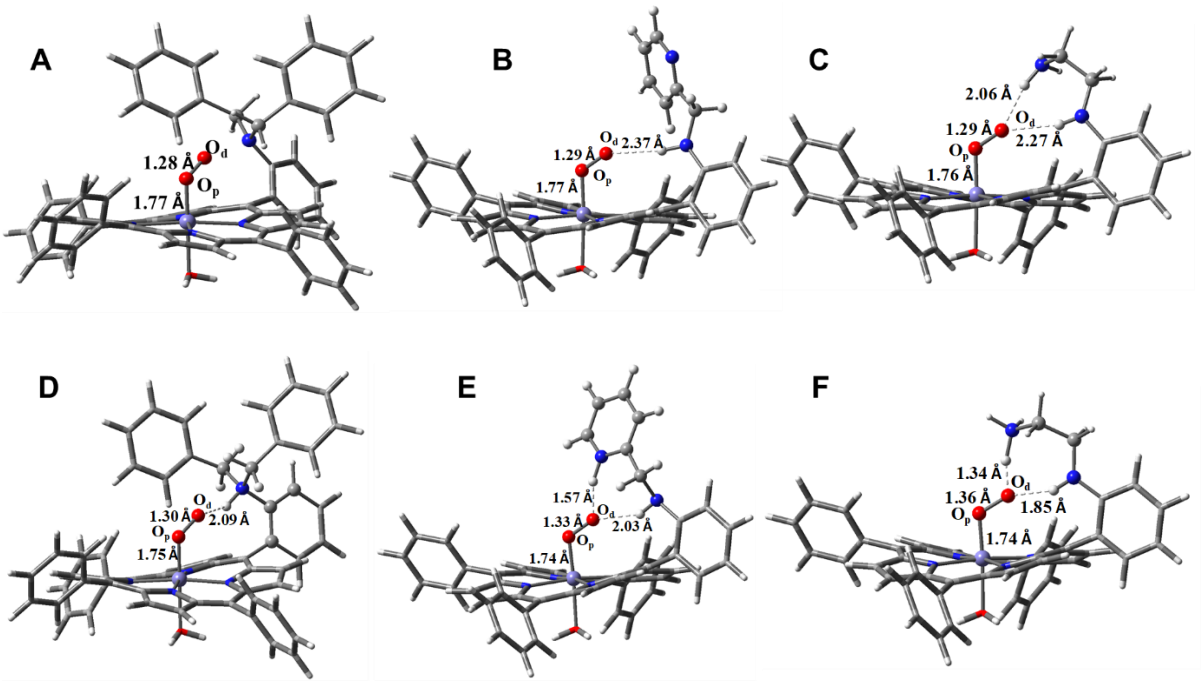

Figure 7. Optimized structures of six-coordinated (A) Fe^{III}L1-superoxide; (B) Fe^{III}L2-superoxide; (C) Fe^{III}L3-superoxide; (D) [Fe^{III}L1-superoxide]H^+ ; (E) [Fe^{III}L2-superoxide]H^+; (F) [Fe^{III}L3-superoxide]H^+ having water as axial ligands and deprotonated basic residues. color codes: carbon → grey, hydrogen→ white, nitrogen → blue, oxygen → red, and iron → bluish grey.

The optimized structures of the low spin Fe^{III}-O_2^- species for FeL1, FeL2 and FeL3 show hydrogen bonding interactions between the distal oxygen atom of the bound superoxide anion and the distal amine groups (Figure 7). In ferric-superoxides, the Fe(III) centre and oxygen are found to be antiferromagnetically coupled from their respective spin densities (Table S6). However, no substantial effect of the hydrogen bonding interaction is observed in the optimized Fe-O and O-O bond lengths of the Fe^{III}-O_2^- species. The optimized structures of the Fe^{III}-O_2^- species where the pendant nitrogen bases are protonated show only slight elongation of the O-O bond lengths in FeL1 (Figure 7D), FeL2 (Figure 7E) and FeL3 (Figure 7F). The hydrogen bonding occurs between the distal oxygen atom of the bound superoxide. It is important to note that the pK_a of free superoxide ion in water is 4.5.[69,70] On binding to the metal, the pK_a will be lowered further. Thus, the protonation of the bound superoxide is not likely to occur at pH 7 where the heterogeneous experiments were performed. However, in an organic solvent with protonated DMF, this protonation is likely and has been demonstrated.

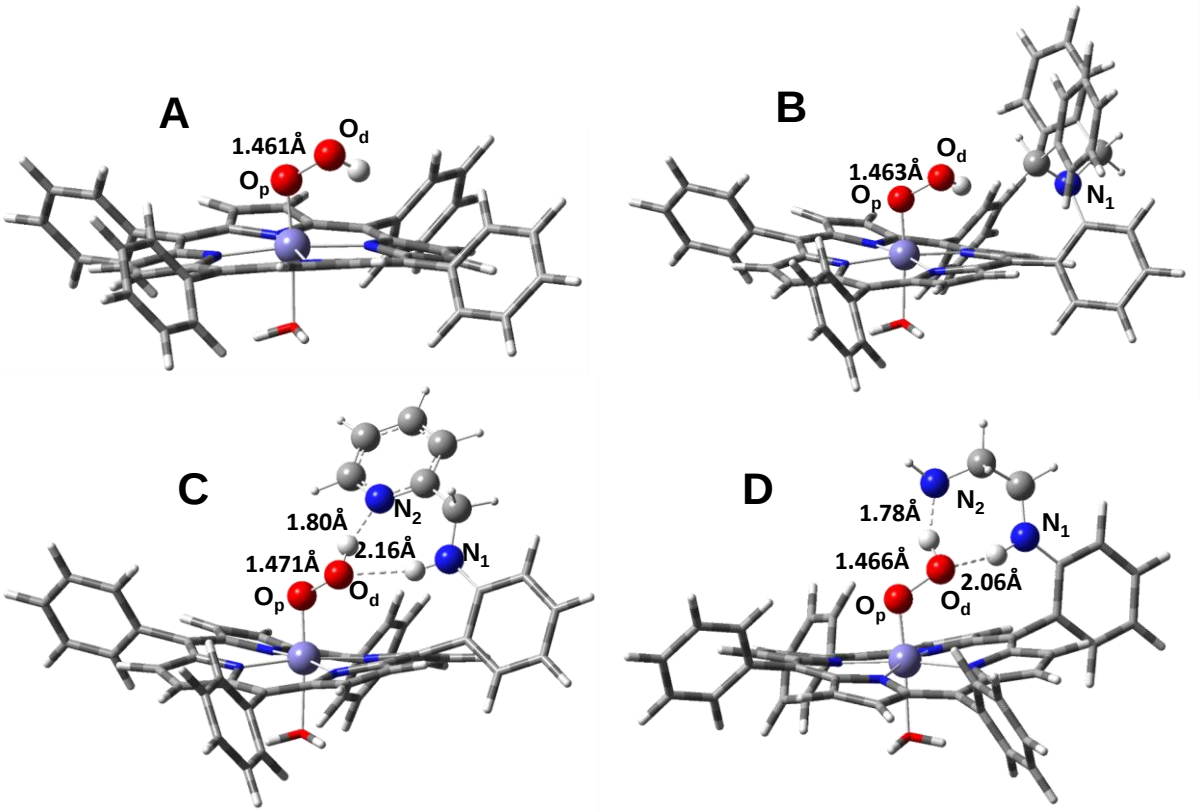

Figure 8. Optimized structures of (A) Fe^{III}TPP-OOH; (B) Fe^{III}L1-OOH; (C) Fe^{III}L2-OOH; (D) Fe^{III}L3-OOH with hydroperoxide and water as axial ligands. *color codes*: carbon → *grey*, hydrogen→ white, nitrogen → *blue*, oxygen → *red*, and iron → *bluish grey.*

All known ferric hydroperoxides reported to date, both in solution and on electrode surfaces, have a S=1/2 low spin ground state.[48,71-73] The six coordinate low spin hydroperoxide model complexes are found to be energetically more stable from DFT optimised structures than their corresponding high spin states which are unlikely to exist (Table S5). It must be noted that DFT is not very reliable with relative spin state energies.[74] The optimized structure of low spin Fe^{III}L1-OOH shows very weak interaction with the N_1H group of the N,N-dibenzyl substituent (Figure 8B). The O-O bond distance in B is 1.46 Å which is slightly longer than that of free H_2O_2 and also similar to that of Fe^{III}TPP-OOH (Figure 8A). The hydrogen bonding is much stronger in Fe^{III}L2-OOH. The distal oxygen atom accepts a H-bond from the N_1H substituent on the phenyl ring and donates a H-bond to the pyridyl nitrogen (N_2) (Figure 8C). The N_1---O_d and N_2---O_d distances are (3.14 Å and 2.79 Å) consistent with the presence of H-bonds. This H-bonding results in the elongation of the O-O bond to 1.47 Å in a Fe^{III}L2-OOH species (Table 2). The Fe^{III}L3-OOH shows strong H-bonds as well. Here, the distal oxygen atom accepts a H-bond from the N_1H substituent on the phenyl group and donates a H-bond to

the amine group (N_2) on the ethylamine substituent (Figure 8D). A similar elongation of the O-O bond to 1.47 Å is observed here as well (Table 2). Thus, there are possible H-bonding interactions with the distal OH of the hydroperoxide adducts of all these complexes. These H-bonding interactions lead to the elongation of the O-O bonds in these LS ferric hydroperoxide complex i.e., the O-O bonds are getting activated for cleavage due to selective H-bonding to the distal oxygen atom of the bound hydroperoxide. Note that the O-O bond lengths calculated here (1.47Å) are much longer than those calculated for bridged peroxide of ba_3 CcO from *Thermus Thermophilus* where the O-O bond length is 1.33 Å and the Fe-O bond length is 1.87 Å.[75]

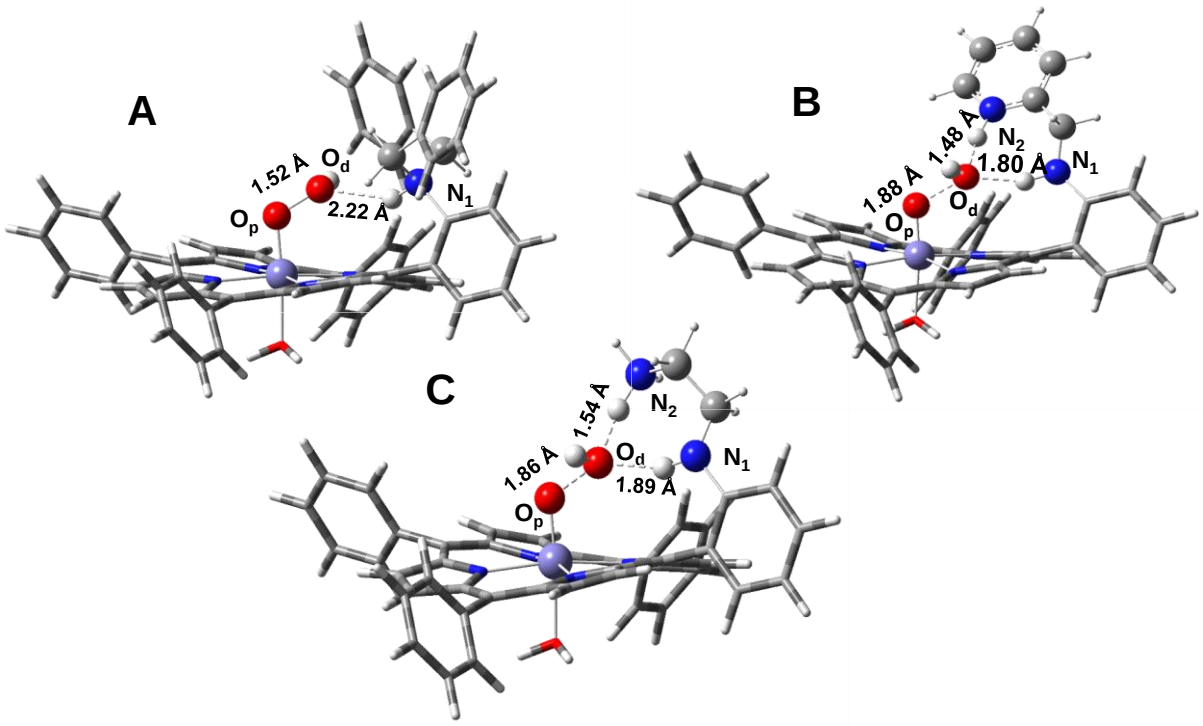

Figure 9. Optimized structures of six coordinate low spin (A) $[Fe^{III}L1\text{-}OOH]H^+$; (B) $[Fe^{III}L2\text{-}OOH]\ H^+$; (C) $[Fe^{III}L3\text{-}OOH]H^+$ with hydroperoxide and water as axial ligands and protonated distal basic residues in PCM model considering water as solvent. *color codes*: carbon → *grey*, hydrogen→ white, nitrogen → *blue*, oxygen → *red*, and iron → *bluish grey.*

The ammine groups have pK_a values around or above 7.0 and can be expected to be protonated at pH 7.0 or in the presence of protonated DMF where the experiments were conducted. The pK_a values of these basic functional groups are enhanced due to strong hydrogen bonding interactions with the distal oxygen atom of the bound hydroperoxide anion. The difference in their pK_a values (ΔpK_a) are obtained from the computed ΔPA (difference

between the proton affinities of basic residues in ferric hydroperoxide and their corresponding free bases) using this correlation: $\Delta pK_a = -\Delta PA/1.36$.[76] The p$K_a$ values are estimated to shift higher by 4-5 units (Table S3) in our cases. The hydroperoxide adducts of these low spin iron porphyrins are optimized with protonated basic residues (Figure 9). In these optimized structures, the hydrogen bonding interactions with the hydroperoxo species are substantially enhanced (Table 2). The $[Fe^{III}L1\text{-}OOH]H^+$ shows remarkable elongation of the O-O bond length to 1.52 Å and is much longer than the deprotonated analogue (1.46 Å). It is hypothesized that a stronger pull effect exists between the distal oxygen atom and the aromatic $\text{-}N_1H^+$ group (Figure 8A). For $[Fe^{III}L2\text{-}OOH]H^+$, the $–N_1H$ group and protonated pyridine (N_2H^+) acts as a H-bond donor to the distal oxygen atom. Like FeL1, the O-O bond length for FeL2 is elongated from 1.47 Å in the deprotonated structure (Figure 8C) to 1.88 Å in the protonated structure (Figure 9B). The same trend also occurs for protonated $Fe^{III}L3\text{-}OOH$, where the protonated aliphatic amine group ($\text{-}NH_3^+$) stretches the O-O bond length to 1.86 Å (Figure 9C). All these optimized geometries suggest that H-bonding to the distal oxygen atom of a $Fe^{III}\text{-}OOH$ species facilitates activation of the O-O bond. The extent of O-O bond elongation is less for $[Fe^{III}L1\text{-}OOH]H^+$ compared to others as the protonated tertiary amine residue is further away from the bound hydroperoxo species relative to FeL2 and FeL3. This resonates well with the slower k_{cat} for the FeL1 complex. Additionally, the optimized geometries show that the proton donor groups are oriented in a way which allows selective delivery of the proton needed to the distal oxygen atom which should aid the heterolytic O-O bond cleavage leading complete O_2 reduction.

Importantly, the elongation of the O-O bond is complemented by shorting of the Fe-O bond. For example, as the O-O bond is elongated from 1.47 Å in $Fe^{III}L2\text{-}OOH$ to 1.88 Å in $[Fe^{III}L2\text{-}OOH]\ H^+$ the Fe-O bond contracts from 1.76 Å to 1.61 Å in $[Fe^{III}L2\text{-}OOH]H^+$. Similar trends are observed, both in geometry and vibrations, in low spin non-heme ferric peroxides.[77] Of course, the shortening of the Fe-O and elongation of the O-O sets up the $Fe^{III}\text{-}OOH$ for cleavage which results in a Fe^{IV}=O species with a much stronger Fe-O bond than the precursor $Fe^{III}\text{-}OOH$.

Table 2: Calculated bond distances and free energies

Catalyst	Hydroperoxide					Hydroperoxide (Protonated residues)			
	$Fe\text{-}O_p$ (Å)	$O_p\text{-}O_d$ (Å)	$O_d\text{-}N_1$ (Å)	$O_d\text{-}N_2$ (Å)	$\Delta G_{hydrolysis}$ (kcal/mol)	$Fe\text{-}O_p$ (Å)	$O_p\text{-}O_d$ (Å)	$O_d\text{-}N_1$ (Å)	$O_d\text{-}N_2$ (Å)
Fe^{III}TPP	1.76	1.46	-	-	8.04	-	-	-	-
Fe^{III}L1	1.76	1.46	3.92	-	11.6	1.75	1.52	3.11	-
Fe^{III}L2	1.76	1.47	3.14	2.79	10.8	1.61	1.88	2.79	2.59
Fe^{III}L3	1.76	1.47	3.04	2.73	14.8	1.64	1.86	2.87	2.63

Discussion

Over the last few years, heterogeneous investigations of the iron-porphyrin based ORR have led to a consensus that the fate of an intermediate Fe^{III}-OOH species is instrumental in controlling both selectivity and rate of the reaction.[39,59,53,52,45] Under some conditions, the rate of O-O bond cleavage of this Fe^{III}-OOH species is thought to be the rate determining step.[46,48] On the other hand the site of protonation of this Fe^{III}-OOH species determine the selectivity.[39] Protonation at the proximal oxygen leads to the release of H_2O_2, the $2e^-/2H^+$ reduction product. Alternatively, protonation of the distal oxygen leads to O-O bond cleavage and $4e^-/4H^+$ ORR.[43,55] Introduction of H-bonding residues in the distal pocket of mononuclear iron porphyrins can both stabilize a Fe^{III}-OOH species and enable selective protonation of the distal oxygen of a Fe^{III}-OOH species activating it for heterolytic cleavage – both of these factors can promote facile and selective $4e^-/4H^+$ O_2 reduction. The mononuclear iron porphyrin complexes, reported here, are fashioned to implement the above design. The amines are chosen such that they all are protonated at pH 7, the basicity of the aromatic amine is not varied rather the basicity of the other appended residue is tuned (pyridine / aliphatic primary amine) and the number of amines is systematically varied.

Accordingly, these complexes exhibit 2nd order rate constants of heterogeneous O_2 reduction which are $>10^7$ $M^{-1}s^{-1}$ surpassing those reported for any synthetic system thus far and matching those reported for sophisticated bio-synthetic scaffolds.[18,29,30,32,78,79] Perhaps more surprising is the >90% selectivity for $4e^-/4H^+$ O_2 reduction exhibited by these set of porphyrins. Such high selectivity for complete reduction of O_2 to water is not generally observed in mononuclear iron porphyrins adsorbed to electrodes.[39,40] This is established by the fact that ROS production does not increase even when the ET rate from the electrode to the catalyst is very slow. In contrast, FeL1 does not follow the same trend where the hydrogen bonding to the bound hydroperoxide is calculated to be the weakest. The experimental results obtained for this complex i.e., the amount of ROS as well as lower rate constant, are also supported by the calculated O-O bond lengths of the optimised structures of putative Fe^{III}-OOH intermediates with protonated distal basic residues. In the past, ET rates of 6-10 s^{-1} to heme/Cu models were emulated by physiadsorbing them on C_{16}-SAM and these systems have been compared to the electron deficient mixed valent state of CcO. The selectivity of O_2 reduction is substantially compromised in these situations as competing hydrolysis of the Fe^{III}-OOH which does not depend on ET, results in H_2O_2 release and mononuclear iron porphyrin complexes rapidly degrade under these conditions (substantial amount of ROS are generated during O_2 reduction).[4,25,30] Under such conditions, only 2nd sphere ET residues like Cu, phenol and Fc have been shown to promote $4e^-/4H^+$ selectivity. The experimental data obtained here clearly show that such 2nd sphere ET residues are not always necessary, and strongly suggest that basic residues capable of H-bonding can also promote the $4e^-/4H^+$ ORR. The facile rates and high selectivity for O_2 reduction imply that these mononuclear iron porphyrins can activate the O-O bond and promote selective protonation to the distal oxygen of the Fe^{III}-OOH intermediate.

A strong correlation between the log(TOF) vs overpotential (η where overpotential is the difference between the thermodynamic potential of ORR and the working potential of the catalyst) of ORR under homogeneous condition with iron porphyrins bearing different substituents in the presence of strong acid has been reported by Mayer and co-workers.[66] The linear relationship between the Fe(III/II) reduction potential $E_{1/2}$, the oxygen binding affinities (pK_{O2}) and pK_a (or proton affinity) of Fe(III)-$O_2^{\cdot-}$ results in linear free energy correlations between the log(TOF) and $E_{1/2}$ of the Fe(III/II) reduction potential. Iron porphyrins with electron donating substituents have more negative Fe(III/II) potentials and generally result in faster TOFs and higher overpotentials for O_2 reduction. When the porphyrin ligand is electron rich, the O_2 binding affinity increases as O_2 binding requires charge transfer from the metal to

O_2. However, such an attempt to correlate the log(TOF) vs η for the complexes reported here did not produce the expected trend i.e., the rate decreases with overpotential (Figure 6). Thus, the enhancement of rate at the same overpotential observed here reflects other factors than solely the primary coordination sphere. Within the smaller subset of catalysts FeL1, FeL2, FeL3, and FeTPP, the four molecules do span multiple orders of magnitude in TOF with little change to the effective overpotential (Figure 6) strongly suggesting the role of 2nd sphere in enhancing rate of ORR. Identifying and detailing the subtle effects in the homogeneous electrochemistry will require further study.

Recently, there has been another proposal from Nocera and co-workers regarding the relationship between selectivity and overpotential where it has been suggested that increased overpotential increases selectivity.[80] However, these conclusions were obtained on a binuclear cobalt complex could not be extrapolated in iron porphyrin systems where $4e^-/4H^+$ selectivity greater than 90% was achieved only in presence of strong acids (homogeneous condition) even at very high potentials.[80] Even the RRDE data presented here do not show such a trend (Figure 4). Overall, the direct comparison and correlation of catalytic activities between molecular ORR catalysts on surfaces and in solution has never been previously reported. Nonetheless, our data demonstrate that these iron porphyrins are among the most active ORR electrocatalysts when adsorbed on electrodes in neutral water media.

Overall, the observations made here emulates the pull effect from basic 2nd sphere residues enhancing O_2 reduction by weakening the O-O bond of Fe^{III}-OOH intermediates, observed in-situ in iron porphyrins, without altering the electronic structure of the iron center. DFT calculations on Fe^{III}-OOH species clearly support this hypothesis. Indeed, the optimized geometries show that the bound hydroperoxide is stabilized by H-bonding to the distal amine residues (Figure 7, 8). Protonation of the amines result in achieving a) substantial elongation of the O-O bond (Table 2) i.e., greater activation of the hydroperoxide and b) selective delivery of the proton to the distal oxygen atom of the Fe^{III}-OOH species i.e., greater selectivity for $4e^-/4H^+$ O_2 reduction (Figure 8 and Table 1). The greater rate and higher selectivity for $4e^-/4H^+$ O_2 reduction observed for complexes FeL2 and FeL3 relative to FeL1 is consistent with the longer O-O bond lengths and better H-bonding i.e., better activation of the O-O bond for cleavage in the proposed Fe^{III}L2-OOH and Fe^{III}L3-OOH species relative to Fe^{III}L1-OOH species (Table 2).

Conclusion

Mononuclear iron porphyrins with distal basic residues, when adsorbed to electrodes, have been shown to selectively reduce O_2 to H_2O (ca. >90%) at pH 7 under rate limiting electron transfer conditions. The rates of O_2 reduction are ca. 100 times faster than previous reports on heme/Cu systems. These results strongly suggest that the distal basic residues a) hydrogen bond to intermediate Fe^{III}-OOH species and stabilize them against deleterious hydrolysis, b) activate the O-O bond of such hydroperoxide species via a "pull effect" and c) promote proton transfer to the distal oxygen.

Experimental Details

All reagents were purchased from commercial sources. Benzyl bromide, Bromo ethylene amine hydrobromide, tetrabutyl ammonium iodide (TBAI), pyridine 2-carboxaldehyde, anhydrous $FeBr_2$ and 2,4,6-collidine were purchased from Sigma-aldrich chemical company. All solvents, triethylamine and Na_2SO_4 were purchased from MERCK and used without further purification. Unless otherwise mentioned solvents were distilled, dried and deoxygenated for using in the glove box. Preparation and handling of air-sensitive materials were carried out under an inert atmosphere in the glove box. Unless otherwise mentioned all reactions were performed at room temperature and column chromatography were performed on silica gel (60-120 mesh), neutral and basic alumina. Elemental analyses were performed on a PerkinElmer 2400 series II CHN analyser. Electro-spray ionisation (ESI) mass spectra were recorded with a Waters QTOF Micro YA263 instrument. The absorption spectra are measured in the SHIMADZU spectrograph (UV-2100). Room temperature ^{1}H-NMR spectra were collected on a Bruker DPX-500 spectrometer. X-ray single crystal data was collected at 120 K and 298K using radiation on a Bruker SMART APEX diffractometer equipped with CCD area detector using graphite monochromatic Mo Kα (λ = 0.71073 Å) radiation. Data collection, data reduction, structure solution refinement was carried out using the software package of APEX II. The structure was solved by direct method and refined in a routine manner. The nonhydrogen atoms were treated anisotropically. All the hydrogen atoms were located on a difference Fourier map and refined.

Electrochemical Measurements (Heterogeneous)

Cyclic Voltammetry:

The cyclic voltammograms (CV) are recorded on a CH Instrument potentiostat model 710D. A 2 mm diameter glassy carbon electrode was used as a working electrode. A Pt wire

was used as a counter electrode. The measurements were made against an Ag/AgCl (saturated KCl) aqueous reference electrode with scan rates varying from 50 mV/s to 500 mV/s.

Electrode Modification:

Physiabsorption on EPG:

A 50 μL portion of catalyst from a 1 mM solution of the respective catalysts in chloroform ($CHCl_3$) is deposited on a freshly cleaned EPG electrode mounted on a RDE setup. After evaporation of the solvent, the surface was rinsed with $CHCl_3$ and sonicated in ethanol and thoroughly dried with N_2 gas. Finally, the modified electrodes were washed with milli-Q water before using it for electrochemical experiments.

Physiabsorption on Alkane thiol Self Assembled Monolayer:

On freshly cleaned Au disc self-assembled monolayer of C_8SH and C16SH were made and the formation of SAM is confirmed by recording the CV. 50 μL from a 1 mM of the catalyst (in $CHCl_3$) was uniformly distributed on the alkyl thiol SAM. After the $CHCl_3$ had evaporated, the surface was sonicated with ethanol and washed with milli-Q water. The charging current was monitored at potentials where there are no Faradayic currents before and after complex deposition to ensure the integrity of the SAM (Figure S8).

Coverage Calculation:

The coverage of a catalyst on an electrode is estimated by taking the average of the integrated area under the corresponding oxidation/reduction currents of the respective species obtained from their reversible voltammogram. The experiments were repeated three times and average values with standard deviation has been reported. The value can be obtained from the equation: $\Gamma = Q/nFA$ [where Q= integrated area under the reduction/oxidation current in coulomb, n= no of electron involved in the process (n=1), F= 96500 C and A= microscopic area of the disk (0.096 cm2)]

Rotating Disc Voltammetry:

The RDE measurements were performed on a CHI 710D bi-potentiostat with a Pine Instruments modulated speed rotor fitted with an E6 series Change-disc tip. The graphite surface was cleaned by polishing it uniformly on a Silicon carbide grinding paper. The complex was physiadsorbed on the disc as described above. The RDE experiment were carried out by

measuring LSV at 100 mV/s scan rate at different rotation rates using Ag/AgCl (saturated KCl) reference and Pt counter electrodes.

Rotating Ring Disk Electrochemistry (RRDE): Reactive Oxygen Species (ROS) Detection and Calculation.

The platinum ring was polished by alumina powder (grit sizes: 1 μ, 0.3 μ, and 0.05 μ) and electrochemically cleaned and inserted into the RRDE tip which is then mounted on the rotor and immersed into a cylindrical glass cell equipped with Ag/AgCl reference (saturated KCl) and Pt counter electrodes. In this technique, the potential of the disk is swept from positive to negative and when O_2 is reduced, any H_2O_2, i.e., a $2e^-$ reduction product of O_2, produced in the working disk electrode is radially diffused to the encircling Pt ring, which is held at a constant potential of 0.7V and oxidizes the H_2O_2 back to O_2. The ratio of the $2e^-/2H^+$ current (corrected for collection efficiency) at the ring and the catalytic current at the disk is expressed as ROS and it provides an in-situ measure of the $2e^-/2H^+$ reduction side reaction. The collection efficiency (CE) of the RRDE setup is measured in a 2 mM $K_3Fe(CN)_6$ and 0.1 M KNO_3 solution at 10 mV/S scan rate and 300 rpm rotation speed. A 19 ± 1% CE is generally recorded during these experiments. The potential at which the ring is held during the collection experiments at pH 7 for detecting H_2O_2 is 0.7 V. The ROS are generally determined at potentials where the Pt ring current is maximum. In the case of $C_{16}SH$ the ROS are determined at -400 mV vs Ag/AgCl (satd. KCl) or -200 mV vs NHE.

Electrochemical measurements (Homogeneous):

Cyclic voltammetry measurements of homogeneous, non-aqueous solutions containing FeL1, FeL2, and FeL3 were all collected on CH Instruments (CHI) model 600D/650D potentiostats using a three-electrode configuration. Glassy carbon (3mm, CHI), platinum wire and silver wire pseudo-reference electrodes were used as the working, auxiliary and reference electrodes, respectively. The Ag/Ag^+ pseudo-reference was prepared by sanding a silver wire and immersing it in a capillary containing 0.1 M $[^nBu_4N][PF_6]$ DMF solution, which was separated from bulk solution by a Vycor tip. All CVs were internally referenced to ferrocene and were corrected for uncompensated resistance (< 2 mV shift in the current-potential response under catalytic conditions) prior to analysis. As previously reported,[66] Foot-of-the-Wave Analysis (FOWA)[81] was used to analyze the data and obtain values for k_{obs}. For all catalysts and under all conditions, the FOWA plots were linear and yielded first-order dependences on [HDMF]OTf.

Salt metathesis to make the triflate analogues of iron(III) porphyrins was accomplished by a stoichiometric addition of thallium triflate to a solution of iron(III) porphyrin chloride dissolved in DMF. The triflate salts were generated in situ preceding electrochemical study by the addition of TlOTf (1M, 20 μL) in DMF and [H-DMF][OTf] (2 M, 12.5 μL) in DMF to a solution of the iron(III) porphyrin chloride and electrolyte in DMF. The presence of a proton source in solution upon halide abstraction prevented Fe-O-Fe dimer formation. In a typical experiment, 0.3 mM catalyst was dissolved in a 0.1 M [$^{n}Bu_4N$][PF_6] DMF solution containing ~ 1 mg ferrocene. Prior to use, the working electrodes were vigorously polished on a felt pad wetted with 0.05 μm alumina slurry before being rinsed with water and DMF. The working electrode was re-polished between scans and yielded reproducible CVs. For kinetic measurements, each catalytic CV was repeated 3x to yield an average k_{obs} value.

1. Dibenzyl substituted monoamino zinc porphyrin (ZnL1):

To a solution of **MAPP** (100mg, 0.159mmol) in 25ml THF, $Zn(OAc)_2.2H_2O$ (58mg, 0.316mmol) was added and the reaction stirred for 6hr. The solvent was evaporated and extracted with DCM and water. After work up the organic layer was collected and dried over anhydrous Na_2SO_4. Finally, purple coloured solid compound (**ZnMAPP**; 1b) was isolated. Then ZnMAPP (50mg, 0.072mmol) was dissolved in Benzyl bromide medium (1ml) at room temperature and stirred overnight. Then, triethyl amine (40μl, 0.290mmol) was added to the reaction mixture for complete conversion by keeping in an ice bath and stirred for 6hr. Then the final mixture was worked up with DCM and water and was dried over anhydrous Na_2SO_4 and evaporated using a rotary-evaporator and purified by column chromatography on neutral alumina with 50% DCM-Hexane mixture as the eluent. Violet coloured compound was isolated (**ZnL1**, 1c; Scheme 2). Yield: (124mg, 90%); Elemental analysis calculated (%) for [ZnL1] ($C_{68}H_{61}ZnN_5O_3$): C 76.93, H 5.79, N 6.60; Found: C 77.59, H 5.80, N 6.37; ^{1}H NMR (500 MHz, $CDCl_3$, 25°C): δ, ppm = 9.10 (m, 8H), 8.41 (m, 7H), 7.84 (m, 8H), 7.75 (t, 2H), 7.58 (t, 1H), 7.41 (d, 1H), 6.81 (t, 2H), 6.70 (t, 4H), 6.43 (d, 4H), 3.6 (s, 4H); UV-Vis (CH_2Cl_2): λ_{max} = 425nm, 551nm, 591nm ; ESI-MS (positive ion mode in ACN): *m/z* (%)= 872.06(100) $[ZnL1]H^+$

2. Dibenzyl substituted monoamino porphyrin (L1):

At first the compound ZnL1 (100mg) in 15ml DCM added to 10ml 6(M) HCl and the reaction was stirred for 5hr. Then the reaction was neutralized by aq. NH_3 solution followed by addition of water and DCM. Then the organic layer was collected and dried with anhydrous

Na_2SO_4. The solvent was evaporated to isolate solid purple colored compound (**L1**, 1d; Scheme 2). Yield: (88 mg, 95%); 1H-NMR (500MHz, $CDCl_3$, 25°C): δ, ppm = 9.07 (m, 8H), 8.41 (m, 6H), 7.83 (m, 11H), 7.65 (d, 1H), 7.43 (d, 1H), 7.09 (t, 2H), 6.98 (t, 4H), 6.64 (d, 4H), 3.7 (s, 4H), -2.31 (s, 2H); UV-Vis (CH_2Cl_2): λ_{max} = 422nm, 518nm, 544nm, 595nm, 653nm ; ESI-MS (positive ion mode in ACN): *m/z* (%)= 809.92(100) $[L1]H^+$.

3. Dibenzyl substituted monoamino iron porphyrin (FeL1):

The ligand (50mg, 0.061mmol) was dissolved in dry degassed THF and about 16 µl of collidine was added to it and stirred for 5 mins. Then $FeBr_2$ (52.46mg, 0.244mmol) was added to the solution and stirred overnight. After the completion of the reaction the solvent was removed and the reaction mixture was worked up with DCM and water after treating with dil HCl to remove excess $FeBr_2$. The organic layer was dried with Na_2SO_4 and evaporated through a rotary evaporator. The reddish brown colored solid was isolated (**FeL1**, 1; Scheme 2). Yield: (50.61 mg, 95%); Elemental analysis calcd (%) for [FeL1] ($C_{64}H_{55}FeN_5Br$): C 74.64, H 5.38, N 6.80; Found: C 76.47, H 5.03, N 7.20; ^{1}H NMR (500 MHz, $CDCl_3$, 25°C): δ, ppm = 80.37 (pyrollic protons), 12-15 (meta hydrogens of phenyl rings of the porphyrin); UV-Vis (CH_2Cl_2): λ_{max} = 419nm, 512nm, 587nm, 687nm ; ESI-MS (positive ion mode in ACN): *m/z* (%)= 862.55(100) $[Fe^{III}(L1)]^+$

4. Methyl pyridine substituted monoamino porphyrin (L2):

To 20 ml a solvent mixture of THF-acetonitrile (1:3), **MAPP** (50mg, 0.079mmol) was added. Then, pyridine 2-carboxaldehyde (30µl, 0.316mmol) and trifluoroacetic acid (28µl, 0.371mmol) were added to the solution and turned green. After 2hr, 5 equivalent of $NaBH_4$ (16mg, 0.417mmol) was added to the reaction and was further, stirred for 12 hr. The colour again changed to reddish brown. The solvent was removed through rotary evaporator and the compound was extracted with dichloromethane. The organic layer was dried with Na_2SO_4 and the solvent was evaporated to isolate the compound. Then the desired compound was eluted with 2% DCM-MeOH mixture through column chromatography using silica gel (60-10 mesh) and reddish brown coloured solid was isolated (**L2**, 2a, Scheme 2). Yield: (40 mg, 70%); ^{1}H NMR (500 MHz,$CDCl_3$, 25°C): δ, ppm = 9.01 (m, 8H), 8.33 (d, 7H), 8.01(m, 1H), 7.83(m, 9H), 7.66(t, 1H), 7.52(t, 1H), 7.23(m, 2H), 7.05(m, 2H), 4.42(s, 2H), 4.25(s, NH), -2.55(s, 2H); UV-Vis (CH_2Cl_2): λ_{max}= 418nm, 516nm, 551nm, 591nm, 651nm ; ESI-MS (positive ion mode in ACN): *m/z* (%) = 721.57 (100) $[L2]H^+$

5. Methyl pyridine substituted monoamino iron porphyrin (FeL2):

The ligand (50mg, 0.069mmol) was dissolved in dry degassed THF and about 18µl of collidine was added to it and stirred for 5minutes. Then $Fe^{II}Br_2$ (60mg, 0.276mmol) was also added and stirred, overnight. After the completion of the reaction the solvent was removed and the reaction mixture was worked up with DCM after treating with dil. HCl to remove excess $FeBr_2$. The organic layer was dried over anhydrous Na_2SO_4 and evaporated using a rotary evaporator. The reddish brown colored solid was isolated (**FeL2**, 2; Scheme 2). Yield: (48 mg, 90%); Elemental analysis calcd (%) for [FeL2] ($C_{56}H_{48}BrFeN_6$): C 71.49, H 5.14, N 8.93; Found: C 72.76, H 5.19, N 8.42; ^{1}H NMR (500 MHz, $CDCl_3$, 25°C): δ, ppm = 79.89 (pyrrolic protons), 11-15 (meta hydrogens of phenyl rings of the porphyrin); UV-Vis (CH_2Cl_2): λ_{max}= 416nm, 512nm, 596nm, 694nm. ESI-MS (positive ion mode in ACN): *m/z* (%) = 774.28 (100) [Fe^{III}L2]. Attempts to grow single crystal for FeL2 failed. Hence, ZnL2 was synthesized following the procedure mentioned above for ZnL1 and characterised with ^{1}H-NMR, ESI-MS and absorption spectroscopy.

7. Ethylene amine substituted mono-amino porphyrin (L3):

To the solution of **MAPP** (50mg, 0.079mmol) in 15ml toluene, 2-bromo ethylamine hydrobromide (65mg, 0.318mmol) and catalytic amount of tertiarybutyl ammonium iodide (TBAI) (5.83mg, 0.016mmol) was added to it. Then the resulting mixture was stirred under refluxing condition for 24 hours. Greenish colored precipitate was obtained after the completion of reaction and the solution was filtered to separate the residue. The residue was then washed with water and extracted with dichloromethane. The solvent was evaporated under vacuum after drying over anhydrous Na_2SO_4. Finally, the product was isolated after purification through column chromatography using neutral alumina with 95% $CHCl_3$-hexane mixture (**L3**, 3a, Scheme 2). Yield:(16mg, 30%). ^{1}H NMR (500 MHz, $CDCl_3$, 25°C): δ, ppm =8.91(m, 8H), 8.25(d, 6H), 7.91(dd,1H), 7.77(m, 10H), 7.70(t, 1H), 7.15(m, 2H), 3.08(t, 2H), 2.48(t, 2H), -2.67(s, 2H); UV-Vis (CH_2Cl_2): λ_{max}= 419nm, 517nm, 552nm, 591nm, 648nm; ESI-MS (positive ion mode in CH_3CN): *m/z* (%) = 673.37(100) $[L3]H^+$.

8. Ethylene amine substituted monoamino iron porphyrin (FeL3):

The ligand **L3** (50mg, 0.069mmol) was dissolved in dry degassed THF and about 18µl of collidine was added to it and stirred for 5mins. Then iron bromide ($Fe^{II}Br_2$) (59mg,

0.276mmol) was also added and allowed to stir for overnight. The solvent was evaporated and the reaction mixture was extracted with DCM after treating with dil. HCl to remove excess metal salt. The organic layer was dried over Na_2SO_4 and evaporated using a rotary evaporator. The reddish brown colored solid was isolated (3, Scheme 2). Yield: (48 mg, 90%); Elemental analysis calcd (%) for [FeL3] ($C_{46}H_{38}FeBrN_6O_2$): C 65.57, H 4.55, N 9.97; Found: C 65.62, H 4.28, N 8.91; ^{1}H NMR (500 MHz, $CDCl_3$, 25°C): δ, ppm = 81.41 (pyrrolic protons), 10-12 (meta hydrogens of phenyl rings of the porphyrin); UV-Vis (CH_3CN): λ_{max}= 417nm (Soret band), 510nm, 594nm, 697nm(Q bands); ESI-MS (positive ion mode in ACN): *m/z* (%) = 725.88 (100) $[Fe^{III}L3]^+$

DFT Calculations

The geometry of all compounds is optimized in gradient corrected BP86 Functional in unrestricted formalism using Gaussian 03 version C03. For hydroperoxide models, Fe, N and O atoms are optimised using 6-311G(d) basis set and 6-31G(d) for other all atoms. For the protonated hydroperoxide models all atoms are optimized with 6-311G(d) basis set in a Polarizable continuum model with water.[82,83] In order to determine the pK_a values of distal basic residues, the protonated and deprotonated analogues of free basic functional groups e.g., N,N-dibenzyl aniline, picoline and ethyl amine were optimised using same basis set in a PCM model. An energy minimum is confirmed by performing frequency calculation on the fully optimized structure using the same basis set used for optimization to ensure no imaginary mode is present for all these compounds. The final energy calculations were performed using 6-311+G(d) basis set on all atoms in PCM model using water as a solvent and convergence criterion of 10^{-10} Hartree.[84-86] Gibbs free energies were calculated for hydroperoxide models of individual ligands in their protonated and deprotonated states along with the free bases (Table S3) from the final optimised geometries and frequencies. All the ferric-superoxide geometries have been optimised considering broken symmetry approximation using the same basis set as mentioned above and BP86 functional for all atoms. To obtain the broken symmetry ground state of the Fe-O_2 adducts, first the triplet wave function was obtained from single point (SP) calculation. The broken symmetry singlet ground state could be obtained by performing a singlet calculation using the triplet wavefunction as an initial guess. The geometries were then optimized by vertically shifting the virtual orbitals using the Vshift keyword.

Acknowledgements

This work was funded by the department of science and technology, India (EMR/2016/008063) and Council for Scientific and Industrial Research (CSIR). S.B. and A.R. acknowledge IACS Integrated Ph.D. Programme for fellowship. M.L.P and D.J.M. were supported as a part of the Center for Molecular Electrocatalysis, and Energy Frontier Research Center funded by the U.S. Department of Energy, Office of Science, Office of Basic Energy Sciences. D.J.M. gratefully acknowledges support by a Graduate Research Fellowship from the National Science Foundation. We acknowledge James M. Mayer, Brian M. Koronkiewicz and Catherine F. Wise for the homogeneous electrocatalysis data, its analysis and insightful discussions and scientific comments this manuscript.

Supporting Information

Experimental NMR data, additional cyclic voltammetry and the optimized co-ordinates are available free of charge online at http://pubs.acs.org

References

(1) Cracknell, J. A.; Vincent, K. A.; Armstrong, F. A. *Chemical Reviews* **2008**, *108*, 2439.
(2) Babcock, G. T.; Wikstrom, M. *Nature* **1992**, *356*, 301.
(3) Chance, B. *The Journal of General Physiology* **1965**, *49*, 163.
(4) Collman, J. P.; Decréau, R. A.; Lin, H.; Hosseini, A.; Yang, Y.; Dey, A.; Eberspacher, T. A. *Proceedings of the National Academy of Sciences* **2009**, *106*, 7320.
(5) Kim, E.; Helton, M. E.; Wasser, I. M.; Karlin, K. D.; Lu, S.; Huang, H.-w.; Moënne-Loccoz, P.; Incarvito, C. D.; Rheingold, A. L.; Honecker, M.; Kaderli, S.; Zuberbühler, A. D. *Proceedings of the National Academy of Sciences* **2003**, *100*, 3623.
(6) Ferguson-Miller, S.; Babcock, G. T. *Chemical Reviews* **1996**, *96*, 2889.
(7) Muramoto, K.; Ohta, K.; Shinzawa-Itoh, K.; Kanda, K.; Taniguchi, M.; Nabekura, H.; Yamashita, E.; Tsukihara, T.; Yoshikawa, S. *Proceedings of the National Academy of Sciences* **2010**, *107*, 7740.
(8) Gennis, R. B. *Proceedings of the National Academy of Sciences* **1998**, *95*, 12747.
(9) Svensson-Ek, M.; Abramson, J.; Larsson, G.; Törnroth, S.; Brzezinski, P.; Iwata, S. *Journal of Molecular Biology* **2002**, *321*, 329.
(10) Tsukihara, T.; Aoyama, H.; Yamashita, E.; Tomizaki, T.; Yamaguchi, H.; Shinzawa-Itoh, K.; Nakashima, R.; Yaono, R.; Yoshikawa, S. *Science* **1996**, *272*, 1136.
(11) Proshlyakov, D. A.; Pressler, M. A.; Babcock, G. T. *Proceedings of the National Academy of Sciences* **1998**, *95*, 8020.
(12) Kaila, V. R. I.; Verkhovsky, M. I.; Wikström, M. *Chemical Reviews* **2010**, *110*, 7062.
(13) Collman, J. P.; Ghosh, S.; Dey, A.; Decréau, R. A.; Yang, Y. *Journal of the American Chemical Society* **2009**, *131*, 5034.
(14) Chufán, E. E.; Puiu, S. C.; Karlin, K. D. *Accounts of Chemical Research* **2007**, *40*, 563.
(15) Anson, F. C.; Shi, C.; Steiger, B. *Accounts of Chemical Research* **1997**, *30*, 437.

(16) Chang, C. J.; Loh, Z.-H.; Shi, C.; Anson, F. C.; Nocera, D. G. *Journal of the American Chemical Society* **2004**, *126*, 10013.

(17) Kadish, K. M.; Frémond, L.; Ou, Z.; Shao, J.; Shi, C.; Anson, F. C.; Burdet, F.; Gros, C. P.; Barbe, J.-M.; Guilard, R. *Journal of the American Chemical Society* **2005**, *127*, 5625.

(18) Collman, J. P.; Boulatov, R.; Sunderland, C. J.; Fu, L. *Chemical Reviews* **2004**, *104*, 561.

(19) Mittra, K.; Chatterjee, S.; Samanta, S.; Dey, A. *Inorganic Chemistry* **2013**, *52*, 14317.

(20) Zhang, W.; Lai, W.; Cao, R. *Chemical Reviews* **2017**, *117*, 3717.

(21) Rigsby, M. L.; Wasylenko, D. J.; Pegis, M. L.; Mayer, J. M. *Journal of the American Chemical Society* **2015**, *137*, 4296.

(22) McGuire Jr, R.; Dogutan, D. K.; Teets, T. S.; Suntivich, J.; Shao-Horn, Y.; Nocera, D. G. *Chemical Science* **2010**, *1*, 411.

(23) Liu, C.; Lei, H.; Zhang, Z.; Chen, F.; Cao, R. *Chemical Communications* **2017**, *53*, 3189.

(24) Shi, C.; Anson, F. C. *Journal of the American Chemical Society* **1991**, *113*, 9564.

(25) Samanta, S.; Mittra, K.; Sengupta, K.; Chatterjee, S.; Dey, A. *Inorganic Chemistry* **2013**, *52*, 1443.

(26) Halime, Z.; Kotani, H.; Li, Y.; Fukuzumi, S.; Karlin, K. D. *Proceedings of the National Academy of Sciences* **2011**, *108*, 13990.

(27) Kieber-Emmons, M. T.; Qayyum, M. F.; Li, Y.; Halime, Z.; Hodgson, K. O.; Hedman, B.; Karlin, K. D.; Solomon, E. I. *Angewandte Chemie International Edition* **2012**, *51*, 168.

(28) Boulatov, R.; Collman, J. P.; Shiryaeva, I. M.; Sunderland, C. J. *Journal of the American Chemical Society* **2002**, *124*, 11923.

(29) Collman, J. P.; Decréau, R. A.; Yan, Y.; Yoon, J.; Solomon, E. I. *Journal of the American Chemical Society* **2007**, *129*, 5794.

(30) Collman, J. P.; Devaraj, N. K.; Decréau, R. A.; Yang, Y.; Yan, Y.-L.; Ebina, W.; Eberspacher, T. A.; Chidsey, C. E. D. *Science* **2007**, *315*, 1565.

(31) Collman, J. P.; Fu, L.; Herrmann, P. C.; Zhang, X. *Science* **1997**, *275*, 949.

(32) Collman, J. P.; Decreau, R. A. *Chemical Communications* **2008**, 5065.

(33) Collman, J. P.; Rapta, M.; Bröring, M.; Raptova, L.; Schwenninger, R.; Boitrel, B.; Fu, L.; L'Her, M. *Journal of the American Chemical Society* **1999**, *121*, 1387.

(34) Liu, J.-G.; Naruta, Y.; Tani, F. *Chemistry – A European Journal* **2007**, *13*, 6365.

(35) Adam, S. M.; Garcia-Bosch, I.; Schaefer, A. W.; Sharma, S. K.; Siegler, M. A.; Solomon, E. I.; Karlin, K. D. *Journal of the American Chemical Society* **2017**, *139*, 472.

(36) Miner, K. D.; Mukherjee, A.; Gao, Y.-G.; Null, E. L.; Petrik, I. D.; Zhao, X.; Yeung, N.; Robinson, H.; Lu, Y. *Angewandte Chemie International Edition* **2012**, *51*, 5589.

(37) Mukherjee, S.; Mukherjee, A.; Bhagi-Damodaran, A.; Mukherjee, M.; Lu, Y.; Dey, A. *Nature Communications* **2015**, *6*, 8467.

(38) Samanta, S.; Sengupta, K.; Mittra, K.; Bandyopadhyay, S.; Dey, A. *Chemical Communications* **2012**, *48*, 7631.

(39) Matson, B. D.; Carver, C. T.; Von Ruden, A.; Yang, J. Y.; Raugei, S.; Mayer, J. M. *Chemical Communications* **2012**, *48*, 11100.

(40) Carver, C. T.; Matson, B. D.; Mayer, J. M. *Journal of the American Chemical Society* **2012**, *134*, 5444.

(41) Sinha, S.; Aaron Michael, S.; Blagojevic, J.; Warren Jeffrey, J. *Chemistry – A European Journal* **2015**, *21*, 18072.

(42) Poulos, T. L.; Kraut, J. *Journal of Biological Chemistry* **1980**, *255*, 8199.

(43) Derat, E.; Shaik, S. *The Journal of Physical Chemistry B* **2006**, *110*, 10526.

(44) Berglund, G. I.; Carlsson, G. H.; Smith, A. T.; Szöke, H.; Henriksen, A.; Hajdu, J. *Nature* **2002**, *417*, 463.

(45) Chatterjee, S.; Sengupta, K.; Hematian, S.; Karlin, K. D.; Dey, A. *Journal of the American Chemical Society* **2015**, *137*, 12897.

(46) Sengupta, K.; Chatterjee, S.; Samanta, S.; Dey, A. *Proceedings of the National Academy of Sciences* **2013**, *110*, 8431.
(47) Sengupta, K.; Chatterjee, S.; Dey, A. *ACS Catalysis* **2016**, *6*, 6838.
(48) Sengupta, K.; Chatterjee, S.; Dey, A. *ACS Catalysis* **2016**, *6*, 1382.
(49) Samanta, S.; Das, P. K.; Chatterjee, S.; Sengupta, K.; Mondal, B.; Dey, A. *Inorganic Chemistry* **2013**, *52*, 12963.
(50) Mukherjee, S.; Bandyopadhyay, S.; Chatterjee, S.; Dey, A. *Chemical Communications* **2014**, *50*, 12304.
(51) Sengupta, K.; Chatterjee, S.; Mukherjee, S.; Dey, S. G.; Dey, A. *Chemical Communications* **2014**, *50*, 3806.
(52) Chatterjee, S.; Sengupta, K.; Samanta, S.; Das, P. K.; Dey, A. *Inorganic Chemistry* **2015**, *54*, 2383.
(53) Costentin, C.; Dridi, H.; Savéant, J.-M. *Journal of the American Chemical Society* **2015**, *137*, 13535.
(54) Soper, J. D.; Kryatov, S. V.; Rybak-Akimova, E. V.; Nocera, D. G. *Journal of the American Chemical Society* **2007**, *129*, 5069.
(55) Matsui, T.; Ozaki, S.-i.; Liong, E.; Phillips, G. N.; Watanabe, Y. *Journal of Biological Chemistry* **1999**, *274*, 2838.
(56) Ozaki, S.-i.; Roach, M. P.; Matsui, T.; Watanabe, Y. *Accounts of Chemical Research* **2001**, *34*, 818.
(57) Sono, M.; Roach, M. P.; Coulter, E. D.; Dawson, J. H. *Chemical Reviews* **1996**, *96*, 2841.
(58) Azcarate, I.; Costentin, C.; Robert, M.; Savéant, J.-M. *Journal of the American Chemical Society* **2016**, *138*, 16639.
(59) Chatterjee, S.; Sengupta, K.; Mondal, B.; Dey, S.; Dey, A. *Accounts of Chemical Research* **2017**, *50*, 1744.
(60) Collman, J. P.; Brauman, J. I.; Doxsee, K. M.; Halbert, T. R.; Bunnenberg, E.; Linder, R. E.; LaMar, G. N.; Del Gaudio, J.; Lang, G.; Spartalian, K. *Journal of the American Chemical Society* **1980**, *102*, 4182.
(61) Collman, J. P.; Sorrell, T. N. *Journal of the American Chemical Society* **1975**, *97*, 4133.
(62) Savéant, J.-M. In *Elements of Molecular and Biomolecular Electrochemistry*; John Wiley & Sons, Inc.: New Jersey, 2006.
(63) Chidsey, C. E. D. *Science* **1991**, *251*, 919.
(64) Decreau, R. A.; Collman, J. P.; Hosseini, A. *Chemical Society Reviews* **2010**, *39*, 1291.
(65) Wasylenko, D. J.; Rodríguez, C.; Pegis, M. L.; Mayer, J. M. *Journal of the American Chemical Society* **2014**, *136*, 12544.
(66) Pegis, M. L.; McKeown, B. A.; Kumar, N.; Lang, K.; Wasylenko, D. J.; Zhang, X. P.; Raugei, S.; Mayer, J. M. *ACS Central Science* **2016**, *2*, 850.
(67) Pegis, M. L.; Wise, C. F.; Koronkiewicz, B.; Mayer, J. M. *Journal of the American Chemical Society* **2017**, *139*, 11000.
(68) Wang, Y.-H.; Pegis, M. L.; Mayer, J. M.; Stahl, S. S. *Journal of the American Chemical Society* **2017**, *139*, 16458.
(69) Behar, D.; Czapski, G.; Rabani, J.; Dorfman, L. M.; Schwarz, H. A. *The Journal of Physical Chemistry* **1970**, *74*, 3209.
(70) Bielski, B. H. J.; Allen, A. O. *The Journal of Physical Chemistry* **1977**, *81*, 1048.
(71) Liu, J.-G.; Shimizu, Y.; Ohta, T.; Naruta, Y. *Journal of the American Chemical Society* **2010**, *132*, 3672.
(72) Liu, J. G.; Ohta, T.; Yamaguchi, S.; Ogura, T.; Sakamoto, S.; Maeda, Y.; Naruta, Y. *Angewandte Chemie International Edition* **2009**, *48*, 9262.
(73) de Visser Sam , P.; Valentine, J. S.; Nam, W. *Angewandte Chemie International Edition* **2010**, *49*, 2099.

(74) Scherlis, D. A.; Cococcioni, M.; Sit, P.; Marzari, N. *The Journal of Physical Chemistry B* **2007**, *111*, 7384.
(75) Du, W.-G. H.; Noodleman, L. *Inorganic Chemistry* **2013**, *52*, 14072.
(76) Moser, A.; Range, K.; York, D. M. *The Journal of Physical Chemistry B* **2010**, *114*, 13911.
(77) Lehnert, N.; Ho, R. Y. N.; Que, L.; Solomon, E. I. *Journal of the American Chemical Society* **2001**, *123*, 8271.
(78) Reedy, C. J.; Gibney, B. R. *Chemical Reviews* **2004**, *104*, 617.
(79) Poulos, T. L. *Chemical Reviews* **2014**, *114*, 3919.
(80) Passard, G.; Ullman, A. M.; Brodsky, C. N.; Nocera, D. G. *Journal of the American Chemical Society* **2016**, *138*, 2925.
(81) Costentin, C.; Drouet, S.; Robert, M.; Savéant, J.-M. *Journal of the American Chemical Society* **2012**, *134*, 11235.
(82) Perdew, J. P. *Physical Review B* **1986**, *33*, 8822.
(83) Mennucci, B.; Tomasi, J.; Cammi, R.; Cheeseman, J. R.; Frisch, M. J.; Devlin, F. J.; Gabriel, S.; Stephens, P. J. *The Journal of Physical Chemistry A* **2002**, *106*, 6102.
(84) Noodleman, L.; Han, W.-G. *JBIC Journal of Biological Inorganic Chemistry* **2006**, *11*, 674.
(85) Ullmann, M. G.; Noodleman, L.; Case, D. A. *JBIC Journal of Biological Inorganic Chemistry* **2002**, *7*, 632.
(86) Miertuš, S.; Scrocco, E.; Tomasi, J. *Chemical Physics* **1981**, *55*, 117.

TOC

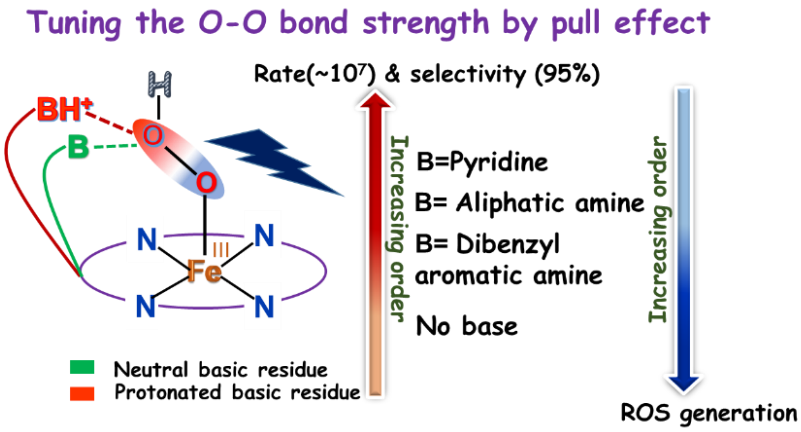
Tuning the O-O bond strength by pull effect
Rate(~10⁷) & selectivity (95%)
BH+
B
H
O
O
N
N
Fe
III
N
N
Neutral basic residue
Protonated basic residue
Increasing order
B=Pyridine
B= Aliphatic amine
B= Dibenzyl aromatic amine
No base
Increasing order
ROS generation